

Supramolecular Approach to Enantioselective DNA Recognition Using Enantiomerically Resolved Cationic 4-Amino-1,8-naphthalimide-Based Tröger's Bases

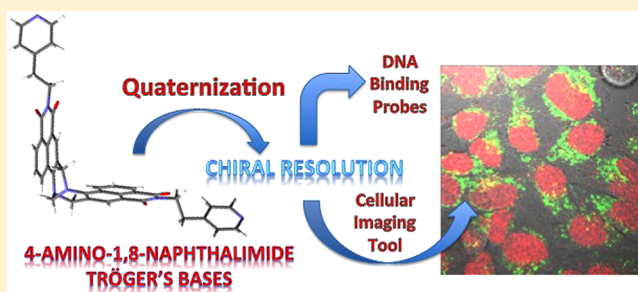
Swagata Banerjee,[†] Sandra A. Bright,[‡] Jayden A. Smith,[†] Jeremy Burgeat,[†] Miguel Martinez-Calvo,[†] D. Clive Williams,[‡] John M. Kelly,^{*,†} and Thorfinnur Gunnlaugsson^{*,†}

[†]School of Chemistry and Trinity Biomedical Sciences Institute, University of Dublin, Trinity College Dublin, Dublin 2, Ireland

[‡]School of Biochemistry and Immunology and Trinity Biomedical Sciences Institute, Trinity College, Dublin 2, Ireland

Supporting Information

ABSTRACT: The synthesis and photophysical studies of two cationic Tröger's base (TB)-derived bis-naphthalimides **1** and **2** and the TB derivative **6**, characterized by X-ray crystallography, are presented. The enantiomers of **1** and **2** are separated by cation-exchange chromatography on Sephadex C25 using sodium (–)-dibenzoyl-L-tartrate as the chiral mobile phase. The binding of enantiomers with salmon testes (st)-DNA and synthetic polynucleotides are studied by a variety of spectroscopic methods including UV/vis absorbance, circular dichroism, linear dichroism, and ethidium bromide displacement assays, which demonstrated binding of these compounds to the DNA grooves with very high affinity ($K \sim 10^6 \text{ M}^{-1}$) and preferential binding of (–)-enantiomer. In all cases, binding to DNA resulted in a significant stabilization of the double-helical structure of DNA against thermal denaturation. Compound (±)-**2** and its enantiomers possessed significantly higher binding affinity for double-stranded DNA compared to **1**, possibly due to the presence of the methyl group, which allows favorable hydrophobic and van der Waals interactions with DNA. The TB derivatives exhibited marked preference for AT rich sequences, where the binding affinities follow the order (–)-enantiomer > (±) > (+)-enantiomer. The compounds exhibited significant photocleavage of plasmid DNA upon visible light irradiation and are rapidly internalized into malignant cell lines.



INTRODUCTION

Supramolecular chemistry has become an important tool in the development of targeting structures for use in recognition, sensing, and imaging of biomolecules and as novel therapeutics. Examples of this class of compound employed in such studies are the Tröger's bases (TB), based on a methano-1,5-diazocine ring, which are cleftlike in structure¹ and commonly formed by reacting an aromatic amine with formaldehyde (or formaldehyde equivalent) in the presence of an acid.² The TB structures are usually formed as racemic mixtures, but the TB is chiral with a C_2 axis of symmetry due to the presence of two stereogenic nitrogen centers.^{2a} In supramolecular chemistry, TB structures have been designed as molecular torsion balances,³ water-soluble cyclophanes,^{2a,b,4} receptors for cations^{5a,b} and anions,^{5c} dicarboxylic acids,⁶ metal-mediated self-assembly systems,⁷ molecular tweezers,^{8a,b} and optoelectronic devices.^{8c} Most of these supramolecules have exploited the "V"-shaped geometry of the TB and have been employed as racemates. Studies with enantiomerically pure TB analogues are relatively limited largely because of the poor availability of the pure enantiomers.⁹ In acidic medium, structurally simple TB derivatives have also been reported to undergo racemization through the formation of an iminium intermediate, which

greatly hinders their application.¹⁰ In recent times, enantiomeric separation of several TB derivatives has been achieved through diastereomeric salt formation using di-*p*-toluoyltartaric acid¹¹ or dibenzoyl-L-tartaric acid.¹² With the advent of chiral stationary phases (CSPs), high-performance liquid chromatography using CSPs also appears to be an attractive method for enantiomeric resolution.¹³ However, surprisingly, only a few examples of enantiomerically pure TBs have been reported to date.

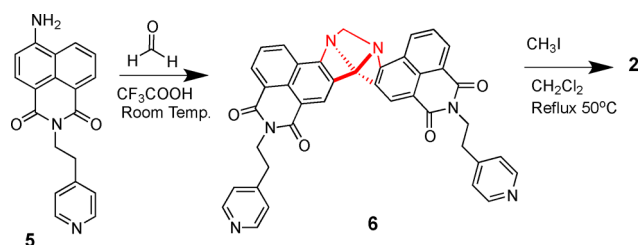
The development of structures that can enantioselectively recognize and target DNA is of great current interest, particularly in supramolecular chemistry, and the TB building motif offers a great opportunity to achieve that due to its unique structure. The introduction of the TB moiety into organic structures can result in a helical structure, or a twist, which can be similar or opposite to the helicity of double-stranded DNA and may therefore result in enantioselective binding. To this end, Yashima et al.¹⁴ have shown that bis-phenanthroline TB derivatives can indeed induce alteration in the secondary structure of DNA compared to the parent 1,10-

Received: July 28, 2014

70 phenanthroline, while Demeunynck and co-workers showed
71 selective DNA binding using bis-acridine-based TB structur-
72 es.^{12a,15a} Further studies from the Demeunynck group using a
73 proflavine-phenanthroline TB derivative also showed that the
74 proflavine moiety can intercalate selectively into DNA, while
75 the phenanthroline unit was found to be a minor groove
76 binder.^{15b} Bhattacharya and co-workers have also recently
77 demonstrated high cytotoxicity and selective binding of bis-
78 benzimidazole-based TB derivatives to guanine quadruplex
79 DNA derived from a human telomeric sequence.¹⁶ Chiral bis-
80 phenanthroline TB analogues have also been incorporated in
81 the design of Ru(II) complexes targeted to B-DNA,¹⁷ but to the
82 best of our knowledge, no other enantiomerically pure TB
83 structures have been developed to date as DNA targeting
84 structures. With this in mind, we set out to develop such
85 examples based on functional luminescent organic structures.

86 Amino-1,8-naphthalimides belong to an important family of
87 DNA binding agents that can display antitumor activities both
88 in vitro and in vivo.¹⁸ Several 3- and 4-amino-1,8-
89 naphthalimide-based DNA targeting and cellular imaging
90 agents have been developed by our research group, and we
91 have also explored their application in luminescent and
92 colorimetric sensing.^{19,20} Recently, we^{20,21} have also reported
93 the development of Tröger's bases incorporating the 4-amino-
94 1,8-naphthalimide moiety,²⁰ and we showed that naphthali-
95 mide-conjugated Ru(II) polypyridyl complexes could also be
96 incorporated into such a TB structure.²¹ To date, however, our
97 efforts have been focused on the use of racemic mixtures of
98 such TB naphthalimide derivatives. We have shown that
99 through careful design they possess good DNA binding affinity
100 and exhibit high cytotoxicity against malignant cancer cell lines.
101 Hence, the amino-1,8-naphthalimide-based TBs are unique
102 supramolecular structures that provide several advantageous
103 photophysical properties, such as strong absorption and
104 emission in the visible wavelength region, due to their internal
105 charge-transfer (ICT) nature.²² In this paper, we present the
106 synthesis and the first examples of enantiomeric resolution of
107 two TB naphthalimide derivatives, namely **1** and **2**, Scheme 2,
108 formed from their corresponding 4-amino-1,8-naphthalimide
109 precursors **3** and **4**. These structures possess alkylpyridinium
110 side chains, which facilitate their interaction with the DNA-
111 phosphate backbone and enhance water solubility. The crucial
112 orthogonal-shaped geometry of these TBs was demonstrated by
113 using solid-state X-ray crystallography of compound **6**, Scheme
114 1, which was initially synthesized as an intermediate for
115 compound **2**. The DNA interactions of **1**, **2**, and their
116 enantiomers were evaluated using salmon testes (*st*)-DNA and
117 synthetic polynucleotides using various spectroscopic methods,
118 and we show that the results demonstrate enantiopreferential
119 recognition of DNA by these TB structures, which were also

Scheme 1. Attempted Synthesis of **2** from **6** via **5**

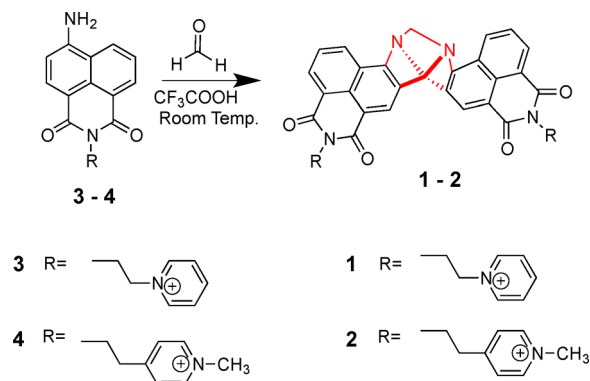


examined for their ability to photocleave plasmid DNA and for
uptake into HeLa cells.

SYNTHESIS AND STRUCTURAL CHARACTERIZATION

The successful syntheses of **1** and **2** are shown in Scheme 2.
Both are based on the use of quaternized pyridine units, which

Scheme 2. Synthesis of TB Derivatives **1** and **2** as Racemic Mixtures



will ensure overall cationic (+2) character for these TB
structures and, hence, water solubility, independent of the
media pH. The two derivatives only differ in the orientation of
their pyridinium moieties relative to the naphthalimide TB
structures.^{19a,b} Originally, our aim was to make compound **2** by
initially forming compound **6**, Scheme 1, and resolve the
enantiomers of **6** prior to the quaternization, which was to be
achieved by methylation of the pyridine ring of **6** to give **2**. The
synthesis of **6** was achieved by reacting compound **5**, also
developed in our laboratory,^{19b} with paraformaldehyde in neat
TFA. During the purification stage, slow evaporation of
compound **6** from CH₂Cl₂ solution yielded crystals that were
of suitable quality for X-ray crystal structure analysis.

The solid-state structure of compound **6** is shown in Figure
1. This is the first example of a solid-state structural analysis of a

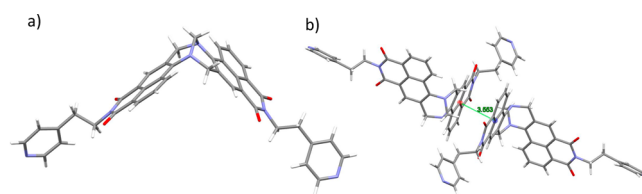


Figure 1. (a) X-ray crystal structure of **6**, showing the orthogonal nature of the two naphthalimide units, forced by the Tröger's base moiety. (b) Packing diagram of **6** when viewed down the crystallographic *b*-axis showing the π - π interaction which is communicated throughout the network (see packing diagrams when viewed down the crystallographic axes *a*, *b*, and *c* in the Supporting Information).

naphthalimide-based TB compound. Compound **6** crystallized
in a monoclinic system, in the centrosymmetric space group
C2/c. The results clearly show that the methano-1,5-diazocine
ring places the two naphthalimide planes almost orthogonal to
each other with an angle of 89.17(5)°. The N-CH₂-N
bridgehead angle for compound **6** is 111.84°, which is within
the range for the same angle in other Tröger's base compounds.

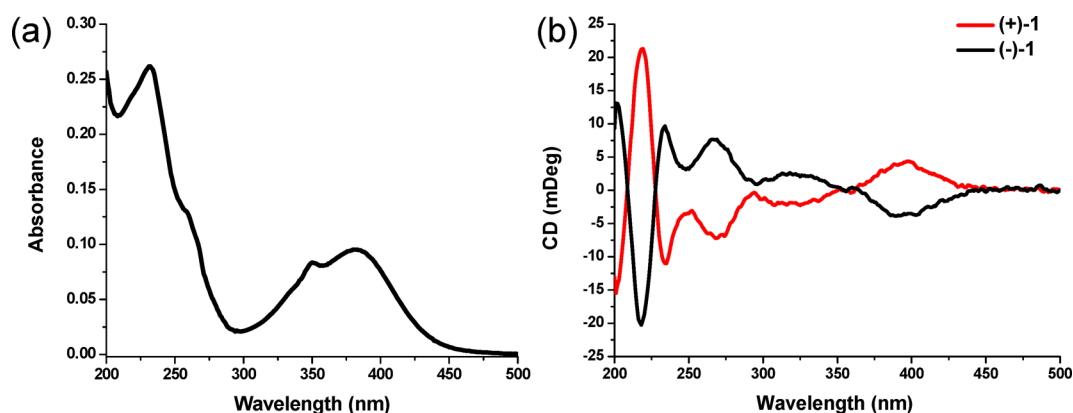


Figure 2. (a) UV/vis absorption and (b) circular dichroism spectra of the (+) and (–) enantiomers of **1** (10 μ M) in 10 mM phosphate buffer (pH 7.0).

148 The molecules pack with pairs of molecules due to the
149 establishment of $\pi\cdots\pi$ stacking interactions between the
150 naphthalimide moieties of two neighboring molecules (d_{centroid}
151 – d_{centroid} 3.553 Å) (see the Supporting Information).
152 Furthermore, CH– π stacking interactions can also be observed
153 in the solid-state packing of **6** between the CH₂ groups of the
154 N–CH₂–N bridgehead and the pyridine group from another
155 neighboring molecule of **6**.

156 Having successfully synthesized **6**, methylation of the two
157 pyridine units was undertaken using CH₃I. However, while the
158 correct product was formed, judging from crude ¹H NMR
159 analysis, it was difficult to purify **2** using standard methods such
160 as column chromatography, as the compound degraded on the
161 column during the purification process, giving naphthalimide
162 byproducts that were difficult to separate from the TB.
163 Consequently, it was necessary to devise a new synthetic
164 route for the desired compound **2** which involved using the
165 quaternized pyridinium starting material **4**. Compound **4** had
166 also previously been developed in our laboratory as a DNA
167 binding molecule,^{19a,b} and this structure was found to be stable
168 toward acidic conditions, necessary for the formation of **2**.
169 Similarly, precursor **3** was developed for the synthesis of **1**.

170 Both TB derivatives **1** and **2** were obtained as racemates by
171 reacting, as outlined above, 2 equiv of the precursors **3** or **4**
172 with paraformaldehyde in neat TFA. Upon completion, excess
173 TFA was removed under reduced pressure in the presence of
174 an excess of CH₂Cl₂. The resulting yellow powder was
175 dissolved in CH₃CN and purified on silica gel using a mixture
176 of CH₃CN/H₂O/NaNO₃ (saturated) as the eluent. The TB
177 derivatives **1** and **2** were obtained in 57% and 53% yields,
178 respectively. In both cases, the presence of the diazocine ring
179 was confirmed by the appearance of a well-separated doublet of
180 doublets between 4.64 and 5.17 ppm in the ¹H NMR (see the
181 Supporting Information, Figures S1–S12), assigned to the
182 methylene protons of the diazocine ring, which also reflect the
183 C₂ symmetry of the molecule.

184 The full characterization of **1** and **2** is given in the
185 Experimental Section. The photophysical properties of both
186 compounds were investigated in 10 mM phosphate buffer (pH
187 7.0) solutions. Compound **1** displayed a broad absorption band
188 centered at 382 nm ($\epsilon = 12000 \text{ M}^{-1} \text{ cm}^{-1}$) as shown in Figure
189 2a. Compound **2** also displayed a similar broad band at 380 nm
190 ($\epsilon = 10700 \text{ M}^{-1} \text{ cm}^{-1}$) (Figure S13a, Supporting Information).
191 For both compounds additional sharp bands at 350 nm and
192 high energy $\pi\text{--}\pi^*$ transition bands were observed at lower

wavelengths. The full photophysical analysis of these
compounds is discussed below.

ENANTIOMERIC RESOLUTION OF **1** AND **2**

Having successfully made both **1** and **2**, we embarked on the
separation of their corresponding enantiomers. The separation
of (\pm)-**1** and (\pm)-**2** was achieved using a column chromatographic
technique developed by Keene and co-workers using
Sephadex C25 as the stationary phase and a chiral eluent
sodium (–)-dibenzoyl-L-tartrate as the mobile phase.²³ The
successful resolution and the enantiomeric purity of (\pm)-**1** and
(\pm)-**2** were determined by using circular dichroism (CD)
spectroscopy.²³

The CD spectra of the enantiomers of compound **1** in 10
mM phosphate buffer (pH 7) are shown in Figure 2b and those
of compound **2** are presented in Figure S13b (Supporting
Information). Importantly, enantiomers of both compounds **1**
and **2** were found to be stable in 10 mM phosphate buffer (pH
7.0) and did not undergo racemization over a period of 6
months. This is probably due to the mild separation conditions
used here (aqueous eluent solution at pH 7.0), which does not
promote protonation on the bridgehead nitrogen atoms and
induce racemization, since TB derivatives are prone to undergo
racemization under acidic condition. The absolute configurations
of the enantiomers were tentatively assigned by comparison
with the proflavin-derived TB of known configuration, where the
(+)-enantiomer was assigned to the (S,S) configuration.^{12a} However,
this should be done with caution as the magnitude and sign of the
Cotton effect may change depending on the substituent present on
the aromatic ring. These are the first examples of enantiomerically
pure 1,8-naphthalimide-based TB derivatives to be isolated by
resolution to date.

PHOTOPHYSICAL PROPERTIES

The photophysical properties of the 4-amino-1,8-naphthalimides
depend strongly on the polarity and H-bonding ability of solvents
due to the “push–pull” nature of the naphthalimide chromophore,
originating from the electronic conjugation between the electron-
donating amino substituent at the 4-position and electron-accepting
imide functional groups.²² With increase in solvent polarity,
the fluorescence spectra of (\pm)-**1** and (\pm)-**2** showed significant
red shift in emission and decrease in quantum yield of emission
(see Figure S14 and Table S1 in the Supporting Information), and
both of the compounds were

236 nearly nonemissive in water. These changes are characteristic of
 237 an ICT excited state, and similar trends have been also reported
 238 by Deprez et al.²⁴ and Veale et al.²⁰ for related 4-amino-1,8-
 239 naphthalimide-based TB derivatives. Yuan et al. have explained
 240 the very weak emission of TB derivatives in aqueous solution in
 241 terms of various nonradiative processes such as intramolecular
 242 vibrations, enantiomerization, etc.²⁵ Having investigated the
 243 photophysical properties of these TB structures in various
 244 solvent systems, we next evaluated their ability to recognize and
 245 bind to DNA using both ground- and excited-state spectroscopy.
 246

247 ■ DNA BINDING INTERACTIONS

248 **UV/vis Absorption Studies.** In the presence of st-DNA
 249 the UV/vis absorption spectra of the TB derivatives (\pm)-1 and
 250 (\pm)-2 showed significant changes. The UV/vis absorption
 251 spectra for (\pm)-1 in the presence of increasing concentrations
 252 of st-DNA are presented in Figure 3. The addition of st-DNA

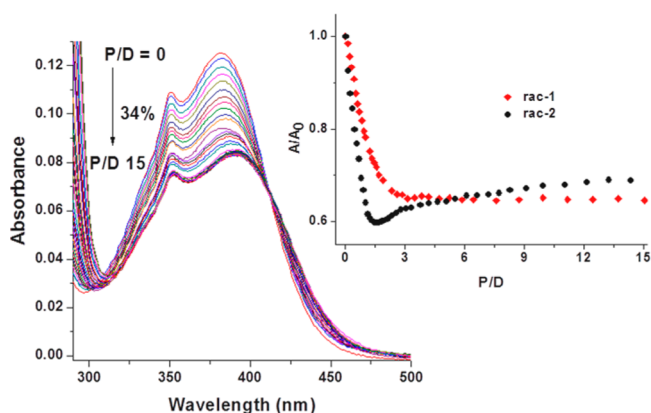


Figure 3. Changes in the UV/vis absorption spectra of (\pm)-1 (10.4 μ M) in the presence of increasing concentration of st-DNA (0–146 μ M) in 10 mM phosphate buffer (pH 7.0). Inset: Plot of relative changes absorbance (A/A_0) vs [DNA base]/[ligand], i.e., P/D for (\pm)-1 (at 382 nm) and (\pm)-2 (at 380 nm).

253 to a solution of (\pm)-1 in 10 mM phosphate buffer (pH 7.0)
 254 resulted in a significant hypochromism (35%) of the absorption
 255 band centered at 382 nm accompanied by a ca. 10 nm red shift
 256 in the λ_{\max} (Table 1). An isosbestic point was observed at 412
 257 nm for all DNA/ligand (P/D ratio) concentrations suggesting
 258 the presence of two distinct species, i.e., free and bound ligand.
 259 In the case of (\pm)-2, with increasing concentrations of st-
 260 DNA, absorbance of the ICT absorption band centered at 380

Table 1. Summary of Binding Parameters Obtained from the UV/vis Titration of (\pm)-1, (+)-1, and (-)-1 with st-DNA in 10 mM Phosphate Buffer (pH 7.0)

	(\pm)-1	(+)-1	(-)-1
λ_{\max} (free) (nm)	382	382	382
λ_{\max} (bound) (nm)	392	390	392
$\Delta\lambda_{\max}$ (nm)	10	8	10
% hypochromism	35	34	36
isosbestic point (nm)	412	418	410
bound P/D	2.5 \rightarrow 15	2.5 \rightarrow 15	2.5 \rightarrow 15
K ($\times 10^6$ M ⁻¹) ^a	1.17 \pm 0.10	1.04 \pm 0.14	1.29 \pm 0.21
n (bp)	0.32 \pm 0.01	0.25 \pm 0.01	0.60 \pm 0.01

^aBinding constant determined using the Bard model.

nm initially decreased by ca. 40% up to P/D of 2 accompanied
 by a 10 nm bathochromic shift in the λ_{\max} . However, with
 further increase in DNA concentrations (P/D 2–15), the
 absorbance of this band increased by ca. 15% without any
 further shift in the λ_{\max} (Figure 4 inset and Figure S15,
 Supporting Information). In 10 mM phosphate buffer (pH
 7.0), both the enantiomers of (\pm)-1 and (\pm)-2 were found to
 bind strongly to DNA and exhibited spectroscopic changes
 similar to those observed for the racemic compounds (see the
 Supporting Information, Figures S16 and S17 and Table S3).

The interactions of (\pm)-1, (\pm)-2, and their enantiomers with
 st-DNA were also investigated at higher ionic strength in the
 presence of 50 and 150 mM NaCl. At higher ionic strengths,
 the overall changes in the absorption spectrum of (\pm)-1 were
 similar to those recorded at low ionic strength; however, the
 extent of hypochromism was ca. 35% in the presence of 50 mM
 NaCl (see the Supporting Information, Figure S18a and Table
 S4) and 29% in the presence of 150 mM NaCl, respectively
 (see the Supporting Information, Figure S18b and Table S5),
 with the changes in absorbance plateauing at higher P/D ratios
 (P/D = 10 \rightarrow 30 in 50 mM NaCl and P/D = 35 \rightarrow 100 in
 150 mM NaCl, respectively).

At higher ionic strength, the degree of hypochromism
 observed for the enantiomers of 1 differed significantly. In the
 presence of 50 mM NaCl, the hypochromism for the 382 nm
 absorption band was found to be greater for the (-)-1
 enantiomer (38%) compared to the (+)-1 enantiomer (31%)
 upon addition of st-DNA with the changes leveling at P/D = 7
 for (-)-1 and P/D = 12 for (+)-1, respectively (see the
 Supporting Information, Figure S18c). The enantiomeric
 preference was more pronounced at 150 mM NaCl
 concentration, where the binding constant of (-)-1 was
 found to be about three times higher than that of
 (+)-enantiomer (Figure 4a and Table 2). This behavior was
 also observed in the reverse salt titration of the two
 enantiomers, where the fraction of (-)-1 remained bound at
 physiological concentration of Na⁺ (ca. 150 mM) was higher
 than that of (+)-1 (see Figure 4c,d).

Interactions of (+)- and (-)-2 with st-DNA were also
 investigated in a similar manner in the presence of 50 and 150
 mM NaCl, respectively (see Figure S19, Supporting Informa-
 tion). At higher ionic strengths, the changes observed in the
 UV/vis absorption spectra of both enantiomers were similar to
 that of (\pm)-2. However, in the presence of st-DNA, the
 enantiomers exhibited a significantly different extent of
 hypochromism and bathochromic shifts under these conditions.
 In the presence of 50 mM NaCl, changes in absorbance
 reached a plateau at a P/D = 3 for (-)-2 and a P/D = 5 for
 (+)-2, respectively (see Figure S19c, Supporting Information).
 Additionally, the degree of hypochromism at 380 nm was also
 found to be greater for the (-)-enantiomer (39%) compared to
 the (+)-enantiomer (35%) upon addition of st-DNA, possibly
 indicating greater binding affinity of the (-)-2 toward st-DNA
 under these conditions. These changes are summarized in
 Table S6 (Supporting Information). A similar trend was also
 observed in the presence of 150 mM NaCl, where a greater
 extent of hypochromism was observed for (-)-2 upon addition
 of st-DNA compared to the (+)-enantiomer (Figure 4b).
 Moreover, the changes in absorbance were found to reach a
 plateau at a P/D = 10 for (-)-2, whereas for the
 (+)-enantiomer, the changes leveled off at a P/D = 15. The
 spectral changes for (\pm)-2 and its enantiomers in the presence
 of st-DNA in 10 mM phosphate buffer containing 150 mM

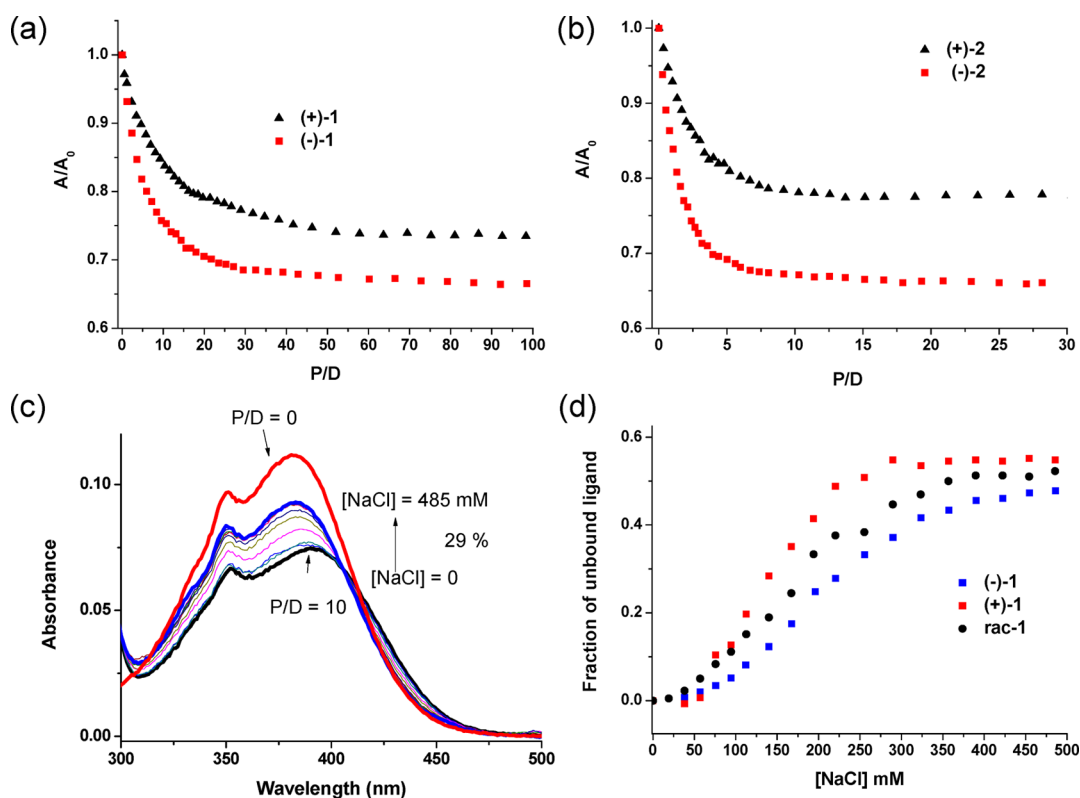


Figure 4. Plot of the changes in the UV/vis absorption spectra of (+)-enantiomer (▲) and (–)-enantiomer (■) of (a) compound 1 and (b) compound 2 in the presence of st-DNA in 10 mM phosphate buffer containing 150 mM NaCl; (c) UV/vis absorption spectra of (±)-1 (9.3 μM) bound to st-DNA (P/D = 10) in 10 mM phosphate buffer (pH 7.0) upon increasing concentrations of NaCl (0–485 mM); (d) fraction of the ligand liberated with increasing concentrations of NaCl.

Table 2. Binding Constants Determined from the Changes in the UV/vis Absorption Spectra of (±)-1, (±)-2, and Their Enantiomers in 10 mM Phosphate Buffer Containing 0, 50, and 150 mM NaCl

$K (\times 10^6 \text{ M}^{-1})^a$	(±)-1	(+)-1	(–)-1	(±)-2 ^b	(+)-2 ^b	(–)-2 ^b
0 mM NaCl	1.17 ± 0.10	1.04 ± 0.14	1.29 ± 0.21	5.31 ± 0.80	5.16 ± 0.68	5.50 ± 0.60
50 mM NaCl	0.73 ± 0.02	0.60 ± 0.02	1.20 ± 0.10	1.10 ± 0.01	0.81 ± 0.07	1.12 ± 0.09
150 mM NaCl	0.20 ± 0.01	0.07 ± 0.005	0.22 ± 0.05	0.74 ± 0.02	0.54 ± 0.05	1.01 ± 0.12

^aBinding constants determined using the Bard model. ^bP/D = 2 data points were fitted to the Bard model.

324 NaCl are summarized in Table S7 (Supporting Information).
 325 The binding constants for the association of (±)-1, (±)-2, and
 326 their enantiomers with st-DNA were determined by analyzing
 327 the changes in absorbance at 382 and 380 nm, respectively, in
 328 the presence of st-DNA using the noncooperative model of (i)
 329 Bard²⁶ and (ii) McGhee and von Hippel.²⁷ In general, the
 330 binding constant analysis suggested that the TB derivatives 1
 331 and 2 have substantially higher affinity (ca. 10^6 M^{-1}) for st-
 332 DNA (see Table 2) compared to their 4-amino precursors (ca.
 333 10^5 M^{-1}).^{19a,b} The binding constant values obtained for 1 and 2
 334 were found to be significantly higher than several acridine-
 335 based antitumor agents.²⁸ Similar binding affinity has also been
 336 reported for other 4-amino-1,8-naphthalimide-based TB
 337 derivatives.²⁰ For both of the compounds, the (–)-enantiomer
 338 displayed markedly higher binding affinity toward st-DNA than
 339 the (+)-enantiomer (Table 2).

340 In all cases, the substantially stronger binding observed for
 341 (±)-2 and its enantiomers compared to (±)-1 presumably
 342 results from the presence of the additional methyl group, which
 343 favors the binding to DNA due to the hydrophobic effect and
 344 which has been previously observed for several other DNA
 345 binders such as Cr(III) complex bearing a dimethyl dpz

ligand,²⁹ dimethylpteridine,³⁰ and 2-amino-1,8-naphthyridine³⁴⁶
 derivatives.³¹ Moreover, the presence of methyl groups can also
 347 increase the polarizability of (±)-2 and consequently allows
 348 better stacking along DNA due to favorable van der Waals
 349 interaction.³² 350

In order to investigate possible sequence-selective binding of
 351 (±)-1 and (±)-2 with DNA, their interactions with
 352 homopolymers poly(dA-dT)₂ and poly(dG-dC)₂ were eval-
 353 uated in a manner similar to that described for st-DNA in
 354 10 mM phosphate buffer containing 50 mM NaCl. Compounds
 355 (±)-1, (±)-2, and their enantiomers were found to interact
 356 strongly with the two polynucleotides as indicated by a marked
 357 decrease in absorbance of the ICT absorption band and
 358 significant red shift in the λ_{max} (the changes in the UV/vis
 359 absorption spectra of (±)-1, (±)-2, and their enantiomers upon
 360 binding to poly(dA-dT)₂ and poly(dG-dC)₂ are shown in
 361 Figure S20–S23, Supporting Information). However, the
 362 extent of hypochromism and red shift were found to be
 363 different for the two enantiomers. As observed previously with
 364 st-DNA, the (–)-enantiomers of both compounds exhibited
 365 higher affinities for the polynucleotides revealed by a greater
 366 degree of hypochromism in the presence of the polynucleotides
 367

Table 3. Binding Constants Determined from the Changes in the UV/vis Absorption Spectra of (\pm)-1, (\pm)-2, and Their Enantiomers in the Presence of Homopolymeric Sequences in 10 mM Phosphate Buffer (pH 7.0) Containing 50 mM NaCl

$K (\times 10^6 \text{ M}^{-1})^a$	(\pm)-1	(+)-1	(-)-1	(\pm)-2	(+)-2	(-)-2
Poly(dA-dT) ₂	0.97 \pm 0.06	0.50 \pm 0.01	1.66 \pm 0.15	3.06 \pm 0.02	1.30 \pm 0.02	4.18 \pm 0.40
Poly(dG-dC) ₂	0.38 \pm 0.01	0.19 \pm 0.02	0.45 \pm 0.01	1.05 \pm 0.03	0.48 \pm 0.02	1.20 \pm 0.03

^aBinding constant determined using the noncooperative model of McGhee and von-Hippel.

with the changes reaching a plateau at a lower P/D than that observed for the (+)-enantiomer (see Figures S20–S23, Supporting Information).

The binding constants of (\pm)-1, (\pm)-2, and their enantiomers for the polynucleotides were estimated from the absorbance changes at the ICT absorption band. These values (Table 3) suggest that both the TB derivatives and their enantiomers display a stronger preference for AT-rich sequences. This is perhaps correlated with the higher negative electrostatic potential of the AT rich minor grooves, which facilitates binding of cationic molecules.³³ Additionally, the minor grooves in the AT rich sequences are narrower than those of GC rich regions, which can possibly allow optimal hydrophobic interactions between the ligand and the grooves and favor binding of these “V”-shaped TB derivatives along the minor groove of DNA.

Ethidium Bromide Displacement Assay. The DNA binding affinity of (\pm)-1, (\pm)-2, and their enantiomers were further investigated using an ethidium bromide (EtBr) displacement assay³⁴ in 10 mM phosphate buffer containing 50 mM NaCl. Changes in the emission spectra of EtBr bound to st-DNA upon titration with (\pm)-1 are shown in Figure 5 (see the Supporting Information, Figure S24, for compound (\pm)-2).

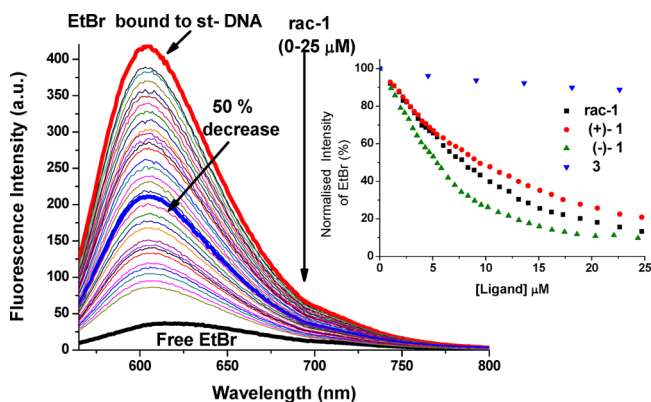


Figure 5. (a) Changes in the emission spectra of EtBr (5 μM) bound to st-DNA, where [EtBr]:[DNA base pair] = 1:2 in the presence of increasing concentrations of (\pm)-1 in 10 mM phosphate buffer containing 50 mM NaCl (pH 7.0); (b) normalized fluorescence intensity of EtBr at 605 nm upon addition of (\pm)-1 (■), (+)-1 (●), (-)-1 (▲), and 3 (▼).

In general, additions of (\pm)-1, (\pm)-2, and their enantiomers resulted in a decrease in the fluorescence of EtBr, demonstrating that these TB derivatives displaced EtBr efficiently. The EC_{50} values (concentration of a ligand required to cause a 50% reduction in the fluorescence intensity of EtBr) and the corresponding apparent binding constants (K_{app}) obtained from the titration of EtBr bound to st-DNA with (\pm)-1, (\pm)-2, and their enantiomers are summarized in Table 4. For comparison, the EC_{50} values determined for the 4-amino-1,8-naphthalimide precursors 3 and 4 are also included

Table 4. EC_{50} Values and K_{app} from the EtBr Displacement Assays in 10 mM Phosphate Buffer Containing 50 mM NaCl (pH 7) ([EtBr] = 5 μM)

compd	EC_{50} (μM)	K_{app} ($\times 10^6 \text{ M}^{-1}$)
(\pm)-1	7.89	0.76
(+)-1	9.45	0.63
(-)-1	5.50	1.09
(\pm)-2	6.00	1.00
(+)-2	6.80	0.88
(-)-2	5.10	1.18
3	79.00	0.08
4	90.00	0.06

in Table 4, which shows that the EC_{50} values are significantly smaller for 1 and 2, and the derived K_{app} values for 1 and 2 were found to be 1 order of magnitude higher than the values obtained for the corresponding 4-amino-1,8-naphthalimide precursors 3 and 4. This trend is in agreement with the higher binding affinity of 1 and 2 determined from the UV/vis titration compared to their precursors 3 and 4 and emphasizes the role of the TB moiety in improving the binding affinity.

Among the TB derivatives, (\pm)-2 was found to be more capable of displacing bound EtBr from st-DNA than compound (\pm)-1. This follows the order of their binding affinity for st-DNA as determined from UV/vis absorption titration. Moreover, for both of the TB derivatives the (-)-enantiomer was found to displace EtBr more strongly than the (+)-enantiomer. This is in accordance with the higher binding affinity of the (-)-enantiomer for both of the TB derivatives.

Thermal Denaturation Studies. To further evaluate the DNA binding affinity of the TB derivatives, thermal denaturation of st-DNA was monitored in the presence of (\pm)-1, (\pm)-2, and their enantiomers. The thermal melting curves in the presence of (\pm)-1, (+)-1, and (-)-1 are shown in Figure 6 (and that in the presence of (\pm)-2 and its enantiomers in Figure S25, Supporting Information). For comparison, the melting curves for the respective precursors 3 and 4 are also included. In the absence of any ligand, the melting temperature (T_m) value for st-DNA was found to be (68 \pm 0.5) $^{\circ}\text{C}$. In the presence of the TB derivatives (\pm)-1 and (\pm)-2 significant stabilization of the double stranded DNA was observed ($\Delta T_m > 7$ $^{\circ}\text{C}$). In fact, the denaturation process was found to be still incomplete at 90 $^{\circ}\text{C}$.

In contrast to these results, only a moderate stabilization was observed for the 4-amino-1,8-naphthalimide precursors 3 and 4 ($\Delta T_m = 4$ –5 $^{\circ}\text{C}$). The high stabilization of DNA in the presence of both TB derivatives correlates with their high binding affinity for st-DNA. Moreover, such a higher extent of stabilization observed for the TB derivatives compared to the 4-amino-1,8-naphthalimide precursors highlights the importance of the rigid “V”-shaped structure of these TB derivatives in stabilizing st-DNA. The thermal denaturation measurements of st-DNA carried out in the presence of the enantiomers of (\pm)-1 and (\pm)-2 showed that both of the (+)- and (-)-enantiomers

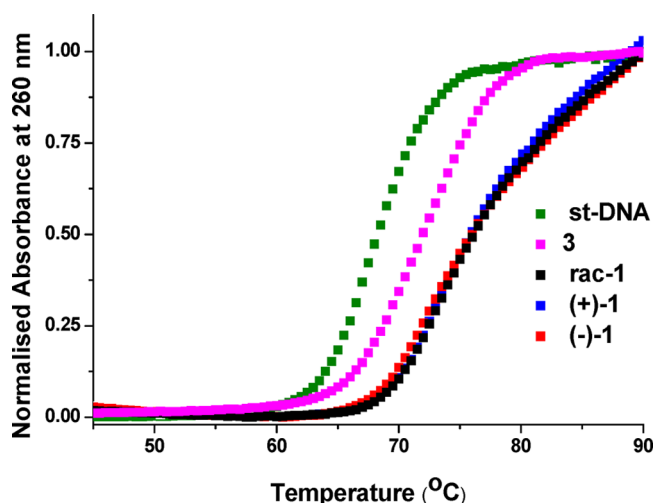


Figure 6. Thermal melting profile of st-DNA (150 μM) in the presence of (\pm)-1, (+)-1, (-)-1 and 3 (P/D 10) in 10 mM phosphate buffer (pH 7.0).

442 stabilized st-DNA to an extent similar to that observed for the
443 racemic mixtures and no significant difference was observed
444 between the enantiomers. This agrees well with the fact that
445 both (+)- and (-)-enantiomers have a comparable high affinity
446 for st-DNA in 10 mM phosphate buffer.

447 **Circular Dichroism Spectroscopy.** CD spectroscopy was
448 further used to monitor the changes in DNA conformation
449 upon binding of the TB derivatives.³⁵ The CD titrations were
450 carried out by monitoring the conformational changes of st-
451 DNA (150 μM) in the presence of increasing concentrations of
452 (\pm)-1 and/or (\pm)-2. The CD spectra of st-DNA in the
453 presence of varying concentrations of (\pm)-1 are shown in
454 Figure 7. The ellipticity of the negative peak centered at 245

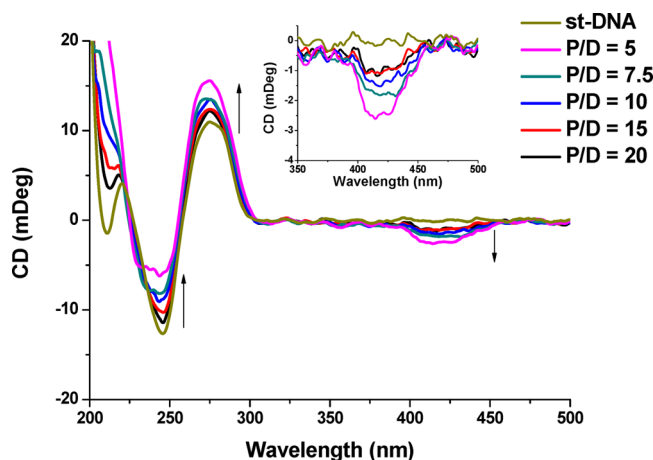


Figure 7. CD spectra of st-DNA (150 μM) in the presence of varying concentrations of (\pm)-1 (P/D 0 \rightarrow 20) in 10 mM phosphate buffer (pH 7.0).

455 nm increased from -14 to -9.0 , while that of the positive peak
456 centered at 275 nm increased from $+12$ to $+16$ mdegree. These
457 changes suggest that (\pm)-1 interacts strongly with st-DNA as
458 has been observed previously for other naphthalimide-based TB
459 derivatives.²⁰ More importantly, a weak negative CD signal was
460 observed at ca. 420 nm as the concentration of (\pm)-1 was
461 raised. Similar induced CD was also observed in the titration of

st-DNA with (\pm)-2 (see the Supporting Information, Figure 462
S26a). Analogous behavior has been previously reported for 463
Ru(II) and Cr(III) complexes, where the appearance of such an 464
ICD signal has been explained due to enantiopreferential 465
binding of one of the enantiomers to DNA.^{29,36} The weak 466
intensity of the ICD signal observed in this case is presumably 467
due to poor enantioselective binding of (-)-enantiomer in low 468
ionic strength buffer. 469

Linear Dichroism Spectroscopy. Linear dichroism (LD) 470
spectroscopy was used to investigate the mode of binding of 471
(\pm)-1 and (\pm)-2 to flow-oriented st-DNA.³⁵ The LD spectra of 472
st-DNA (400 μM) in the absence and in the presence of (\pm)-1 473
(P/D = 10 \rightarrow 30) are shown in Figure 8, respectively. In the 474

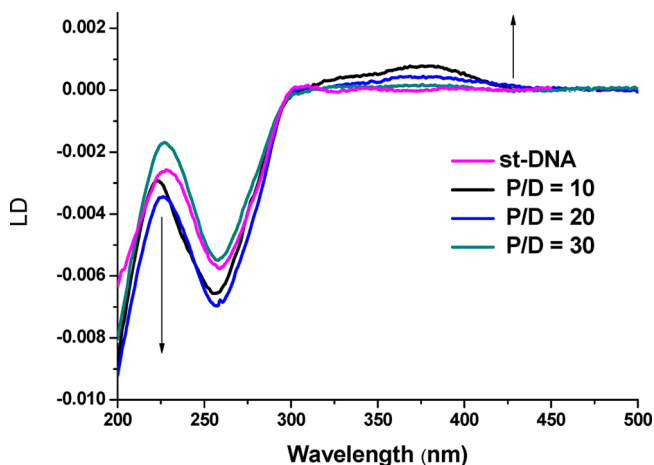


Figure 8. LD spectra of st-DNA (400 μM) in the presence of varying concentrations of (\pm)-1 (P/D 0 \rightarrow 30) in 10 mM phosphate buffer (pH 7.0).

absence of any ligand, a negative LD signal was observed at $\lambda =$ 475
260 nm arising from the nearly perpendicular orientation of the 476
transition moments of the DNA bases relative to the DNA 477
helical axis.³⁵ In the presence of ligand (\pm)-1 and/or (\pm)-2, the 478
LD signal for the 260 nm band was still negative; however, a 479
positive LD signal was observed in both cases around 380 nm 480
corresponding to the ICT absorption band of the compounds. 481
Table 5 summarizes the reduced linear dichroism (LD^r) values 482

Table 5. Summary of LD^r Data for (\pm)-1 and (\pm)-2 in the Presence of st-DNA (error \pm 10%)

	LD^r 260 nm	LD^r 380 nm
st-DNA	-0.022	
st-DNA + (\pm)-1	-0.024	+0.026
st-DNA + (\pm)-2	-0.027	+0.021

for the absorption bands at 260 and 380 nm for (\pm)-1 and 483
(\pm)-2 at P/D ratio of 10, where the ligands should be 484
completely bound to st-DNA. As shown in Table 5, the 485
magnitudes of LD^r value for the DNA absorption region was 486
found to increase slightly in the presence of both (\pm)-1 and 487
(\pm)-2, which is consistent with the stiffening of DNA. 488
Additionally the appearance of positive LD signals in the 489
presence of both (\pm)-1 and (\pm)-2 suggest that the transition 490
dipoles of these ligands are oriented at angles less than 54.7° 491
relative to the helical axis, indicative of binding of (\pm)-1 and 492
(\pm)-2 to the DNA groove. 493

494 ■ DNA PHOTOCLEAVAGE STUDIES

495 In order to investigate the photocleavage abilities of the TB
496 derivatives, pBR322 DNA (1 mg/mL) was treated with the TB
497 derivatives and their precursors and irradiated for 60 min with a
498 Hg–Xe lamp filtered to exclude wavelengths less than 360 nm
499 (Figure 9). When they were incubated with (±)-1 or (±)-2 (P/

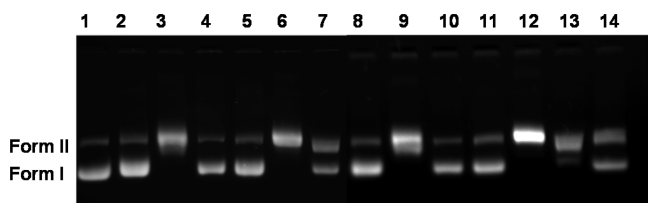


Figure 9. Agarose gel electrophoresis of pBR322 DNA (1 mg/mL) after irradiation at $\lambda > 350$ nm in 10 mM phosphate buffer (pH 7.0). Lane: 1, pBR322 control; 2, 3 (P/D 20) nonirradiated; 3, (±)-1 (P/D 10) nonirradiated; 4, (±)-1 (P/D 10) nonirradiated + extracted; 5, 3 (P/D 20) irradiated; lane 6, (±)-1 (P/D 10) irradiated; 7, (±)-1 (P/D 10) irradiated + extracted; 8, 4 (P/D 20) nonirradiated; 9, (±)-2 (P/D 10) nonirradiated; 10, (±)-2 (P/D 10) nonirradiated + extracted; 11, 4 (P/D 20) irradiated; 12, (±)-2 (P/D 10) irradiated; 13, (±)-2 (P/D 10) irradiated and extracted; 14, reference compound (P/D 20) irradiated.³⁷

500 D = 10) in the absence of light, significant retardation in the
501 mobility of supercoiled DNA was observed (lanes 3 and 9,
502 respectively). This is perhaps due to the dicationic nature of the
503 TB derivative, binding of which results in reduction in the
504 overall negative charge of plasmid DNA and hence caused
505 reduced mobility. To overcome this, samples containing TB
506 derivatives (±)-1 and (±)-2 were extracted with phenol/CHCl₃
507 prior to electrophoresis. The 4-amino precursors 3 and 4 did
508 not induce any significant photocleavage upon photoirradiation,
509 with ca. 18% cleavage being observed (lanes 5 and 11). The
510 failure to observe significant photocleavage activity with the 4-
511 amino analogues is perhaps related to their lower oxidizing
512 potential. In contrast to the 4-amino precursors, the TB
513 derivatives (±)-1 and (±)-2 were found to cause significant
514 (85–90%) photocleavage of the plasmid upon irradiation
515 (lanes 6, 7 and lanes 12, 13, respectively), higher than that
516 observed for unsubstituted 1,8-naphthalimide derivative (ex-
517 hibiting ca. 70% photocleavage, lane 14).³⁷

518 To verify the possibility of covalent adduct formation
519 between the TB derivatives and DNA upon photoirradiation,
520 a solution of st-DNA containing (±)-1 at a P/D = 10 was
521 irradiated for 1 h and subjected to the phenol/CHCl₃
522 extraction. UV/vis absorption spectra of the organic layers of
523 both the irradiated and nonirradiated samples showed the
524 presence of the TB derivative (±)-1 (Supporting Information,
525 Figure S27), suggesting efficient removal of most of the bound
526 ligand from st-DNA. This would not be the case if (±)-1 was
527 irreversibly bound to DNA.

528 ■ CELLULAR UPTAKE STUDIES

529 The cellular uptake and localization studies of (±)-1 and (±)-2
530 in cervical cancer cell lines (HeLa) were carried out using
531 confocal fluorescence microscopy, which demonstrated rapid
532 cellular uptake within 30 min of incubation and apparent
533 localization of the compound within the cytoplasm or at the
534 edge of the nucleus, where the fluorescence presumably arises
535 from the binding of TB derivatives to hydrophobic pockets of
536 proteins or membrane structures (Figure 10).

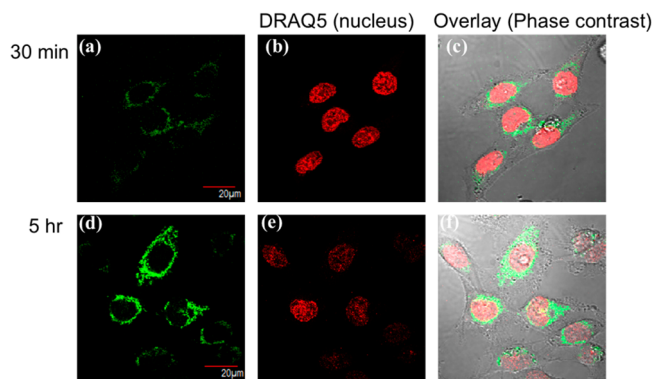


Figure 10. Confocal laser scanning microscopy images of HeLa cells treated with (a) (±)-1 (20 μ M), (b) nuclear stain DRAQ5, (c) overlay of (±)-1 and DRAQ5 (phase contrast) after 30 min of incubation; (d) (±)-1 (20 μ M), (e) nuclear stain DRAQ5, and (f) overlay of (±)-1 and DRAQ5 (phase contrast) after 5 h of incubation.

537 The antiproliferative effects of the compounds were
538 evaluated in HeLa cells using a range of concentrations (1–
539 100 μ M) using an Alamar blue viability assay under dark and
540 light irradiated conditions (Supporting Information, Figure
541 S28). These studies suggest that (±)-1 and (±)-2 possess
542 significant potential as cellular imaging agents. We are currently
543 investigating the biological effects of these compounds in
544 greater detail.

545 ■ CONCLUSION

546 In summary, we have synthesized two novel bis-1,8-
547 naphthalimide-based TB derivatives (±)-1 and (±)-2, which
548 undergo rapid cellular uptake and do not affect cellular viability
549 significantly. We present for the first time a solid-state analysis
550 of the TB naphthalimide structure, which clearly demonstrates
551 the orthogonal nature of the two naphthalimides, forced by the
552 methano-1,5-diazocine ring.

553 The TB compounds were resolved into their enantiomers by
554 cation-exchange column chromatography using a chiral eluent.
555 The TB derivatives (±)-1 and (±)-2 and their enantiomers
556 showed strong affinity for st-DNA (ca. 10^6 M⁻¹) in 10 mM
557 phosphate buffer. The “V”-shaped structure of these TB
558 derivatives presumably exerts steric constraints preventing
559 intercalation of the planar naphthalimide ring. Consequently,
560 the binding site size was found to be significantly less than unity
561 in all cases, suggesting that these molecules bind to the DNA
562 groove and cause significant stiffening of DNA structure.
563 Although our current studies do not provide adequate
564 information regarding the binding of these compounds along
565 major groove or minor groove, strong preference of (±)-1 and
566 (±)-2 and their enantiomers for the AT-rich polynucleotide
567 suggests that these TB derivatives possibly bind to the minor
568 groove of DNA. At low ionic strength buffer, the (+)- and
569 (–)-enantiomers of both 1 and 2 showed comparable DNA
570 binding affinity presumably due to very strong association of
571 the compounds under such conditions. However, at higher
572 ionic strength, the binding affinity of the (–)-enantiomer was
573 found to be greater than that of the (+)-enantiomer for both of
574 the TB derivatives 1 and 2. This enantioselectivity was more
575 pronounced in the presence of 150 mM NaCl, which closely
576 resembles the physiological Na⁺ concentration. This enantio-
577 selectivity probably results from the different three-dimensional
578 shape of the enantiomers, which promotes binding of the
579 (–)-enantiomer to the right-handed B-DNA over the 579

580 (+)-enantiomer. The unique “V”-shaped structure of these TB
581 derivatives combined with their strong affinity for DNA may be
582 used to develop probes for various DNA secondary structures
583 such as “hairpin loop” and “bulged nucleotide sequences”,
584 which play important roles during key physiological events like
585 translational initiation, protein cleavage, mutagenesis, etc., and
586 are therefore considered as important drug-targeting sites. We
587 are currently investigating the mode of binding of these TB
588 derivatives, their ability to recognize specific various secondary
589 nucleic acid structures and the consequent biological effects in
590 detail.

591 ■ EXPERIMENTAL SECTION

592 **General Experimental Details.** All chemicals including salmon
593 testes st-DNA, and homopolymeric sequences and solvents were
594 obtained from commercial sources and used without further
595 purification. The DNA concentration per nucleotide was determined
596 spectrophotometrically using the molar extinction coefficients, $\epsilon_{260} =$
597 $6.6 \times 10^3 \text{ M}^{-1}\text{cm}^{-1}$ for st-DNA, $\epsilon_{254} = 8.4 \times 10^3 \text{ M}^{-1}\text{cm}^{-1}$ for
598 poly(dG–dC)₂, and $\epsilon_{260} = 6.6 \times 10^3 \text{ M}^{-1}\text{cm}^{-1}$ for poly(dA–dT)₂,
599 respectively. In titrations the ratio of nucleotide to naphthalimide is
600 given as P/D.

601 All NMR spectra were recorded using an NMR spectrometer,
602 operating at 400/600 MHz for ¹H NMR and 100/150 MHz for ¹³C
603 NMR, respectively. Chemical shifts were referenced relative to the
604 internal solvent signals. Multiplicities are abbreviated as follows: singlet
605 (s), doublet (d), triplet (t), double triplet (dt). Full assignments of the
606 ¹H NMR peaks for the compounds have been confirmed by measuring
607 ¹³C–¹H HSQC and ¹³C–¹H HMBC COSY experiments. Infrared
608 (IR) spectra were recorded on a FT-IR spectrophotometer equipped
609 with an Universal ATR sampling accessory. Mass spectra of the
610 compounds were recorded either on an electrospray mass
611 spectrometer or a MALDI QToF Premier, using HPLC-grade
612 methanol, water, or acetonitrile as carrier solvents. High-resolution
613 mass spectra were obtained by a peak matching method using leucine
614 enkephaline (Tyr–Gly–Gly–Phe–Leu) as the reference (*m/z* =
615 556.2771). All accurate masses were quoted to ≤ 5 ppm. Melting
616 points were determined using a standard digital melting point
617 apparatus.

618 **Solid-State Analysis.** X-ray data were collected on a diffractometer
619 using graphite-monochromated Mo K α radiation ($\lambda = 0.71073 \text{ \AA}$).
620 Data sets collected on the diffractometer were processed using Bruker
621 APEXv2011.8-0 software. The structures were solved by direct
622 methods (SHELXS-97) and refined against all F₂ data (SHELXL-
623 97). The hydrogen atom positions were included in the model by
624 electronic density or were geometrically calculated and refined using a
625 riding model, CCDC 1007928.

626 **Enantiomeric Resolution Chromatography.** The enantiomers
627 of the TB derivatives were resolved by cation-exchange chromatog-
628 raphy on CM Sephadex C25 as the stationary phase and an aqueous
629 solution of (–)-*O,O'*-dibenzoyl-L-tartaric acid (as its sodium salt) as
630 the chiral mobile phase (pH 7). The concentration of the eluent was
631 adjusted at 0.05 or 0.07 M to achieve better resolution. In each case,
632 the successful resolution of the enantiomers was achieved after three
633 recycles through a 1 m Perspex column fitted to a peristaltic pump,
634 and in each case, the (–)-enantiomer eluted before the (+)-enan-
635 tiomer.

636 **UV/vis Absorption Measurements.** UV/vis absorption spectra
637 were recorded in quartz cuvettes (10 mm \times 10 mm). The wavelength
638 range was 200–800 nm with a scan rate of 600 nm/min. Milli-Q water
639 was used in DNA related work. Phosphate buffer: two 1 M stock
640 solutions of Na₂HPO₄ and NaH₂PO₄ were made up with Milli-Q
641 water. Portions of each solution were diluted together to achieve 10
642 mM phosphate buffer of pH 7.0, which was then filtered using a 0.45
643 μM syringe filter. Baseline corrections were performed for all spectral
644 measurements. All solutions were prepared fresh prior to measure-
645 ment. The UV/vis titrations were carried out by monitoring the
646 changes in the absorption spectra of the ligand of interest in 10 mM

phosphate buffer (pH 7.0) upon gradual addition of mononucleotides/
st-DNA/polynucleotides. All of the titrations were repeated at least
three times to ensure reproducibility.

Fluorescence Measurements. Steady-state fluorescence spectra
were recorded using optically dilute solutions (absorbance <0.1)
following the same procedure as described for UV/vis titrations.
Fluorescence quantum yields of the TB derivatives were
calculated using quinine sulfate in 1 N H₂SO₄ ($\phi_F = 0.546$, $\lambda_{\text{ex}} = 365$
nm) as the reference.³⁸ For determination of the quantum yields, a
number of solutions of the ligand with absorbance ranging from 0.02
to 0.1 were used. Optically matched solutions of the samples and
reference were used. The fluorescence emission spectra of the samples
and the standard were measured under same experimental settings.
The integrated areas under the emission spectra were measured using
the in-built software of the spectrofluorimeter. All the quantum yield
values reported were within 10% error.

Circular Dichroism and Linear Dichroism. CD spectra were
recorded on a spectropolarimeter. Each CD trace represents the
average of three scans. Linear dichroism spectra were recorded on a CD
spectropolarimeter equipped with a linear dichroism accessory. The
LD spectra were presented as the average of three scans.

For an oriented sample, linear dichroism is defined as the
differential absorption of light polarized parallel (A_{par}) and
perpendicular (A_{per}) to a reference axis (eq 1):

$$\text{LD} = A_{\text{par}} - A_{\text{per}} \quad (1)$$

Quantitative information about the orientation of a chromophore
with respect to the reference axis can be obtained from reduced LD
(LD^r) as described in eq 2

$$\text{LD}^r = \frac{\text{LD}}{A} = \frac{A_{\text{par}} - A_{\text{per}}}{A} = \frac{3}{2}S(3 \cos^2 \alpha - 1) \quad (2)$$

where A is the absorbance of the sample under isotropic condition (i.e.,
no orientation), S refers to the orientation factor ($S = 1$ for a perfectly
oriented sample, $S = 0$ for a random orientation), and α is the angle
between the transition dipole of the chromophore and the reference
axis. The magnitude of S provides information about structural
changes in the macromolecule such as lengthening, stiffening, bending
etc.

Thermal Denaturation Assays. Thermal denaturation experi-
ments were conducted on an UV/vis spectrophotometer coupled to a
Peltier temperature controller. The temperature was ramped from 30
to 90 °C at a rate of 1 °C/min rate, and the absorbance at 260 nm was
measured at every 0.2 °C interval. All of the solutions were thoroughly
degassed prior to measurement.

DNA Photocleavage Studies. The DNA photocleavage studies
were conducted by treating the pBR322 plasmid DNA (1 mg/mL)
with the ligand of interest at varying P/D ratios. The samples were
then irradiated for 1 h with an Hg–Xe lamp using a green glass filter
and water IR filter ($\lambda > 350 \text{ nm}$). An equal volume of the buffer
saturated phenol/CHCl₃/isoamyl alcohol (25:24:1) mixture was
added to the irradiated plasmid DNA samples and mixed gently
using a micropipette. The mixtures were centrifuged for 2 min, and
the aqueous layer was carefully removed. The extracted plasmid DNA
samples were mixed with a loading dye solution composed of sucrose
(40%), xylene–cyanol (0.25%), and bromophenol blue (0.25%) and
were then separated using horizontal agarose gel (0.8% w/v) in TBE
buffer (8.9 mM Tris-HCl, 8.9 mM boric acid, and 1 mM EDTA, pH
8.0). Electrophoresis was carried out at ca. 5 V/cm (40 mA, 90 V) to
separate the covalently closed circular (form I), open circular (form
II), and linear (form III) forms of plasmid DNA. The DNA samples
were stained using an aqueous solution of ethidium bromide for 90
min, destained with Milli-Q water and visualized using a trans-
illuminator equipped with a camera. The ratio of the various DNA
forms was estimated using the ImageJ Gel analysis software.

General Biological Procedure. HeLa cells were grown in
Dulbecco's Modified Eagle Medium (Glutamax) supplemented with
10% fetal bovine serum and 50 $\mu\text{g}/\text{mL}$ penicillin/streptomycin at 37
°C in a humidified atmosphere of 5% CO₂.

713 **Alamar Blue Viability Assay.** HeLa cells were seeded at a density of
714 5×10^3 cells/well in a 96-well plate and treated with the indicated
715 compounds for 48 h. Alamar blue (20 μ L) was then added to each well
716 and incubated at 37 °C in the dark for 4 h. Plates were then read on a
717 fluorescent plate reader with excitation and emission wavelengths of
718 544 and 590 nm, respectively. Experiments were performed in
719 triplicate on three independent days with activity expressed as
720 percentage cell viability compared to vehicle treated controls. All
721 data points (expressed as means \pm S.E.M.) were analyzed using
722 GRAPHPAD Prism software.

723 **Confocal Microscopy.** HeLa cells were seeded at a density of $1 \times$
724 10^5 cells/well in glass bottom wells and treated with the indicated
725 compounds for up to 48 h. Cells were washed, followed by the
726 addition of fresh media and DRAQ5 (red nuclear stain), followed by
727 viewing using confocal microscopy with a 60 \times oil immersion lens.
728 Image analysis was performed using FluoView Version 7.1 Software.
729 Compounds were excited by a 405 nm argon laser, emission 480–580
730 nm, DRAQ5 was excited by a 633 nm red helium–neon laser,
731 emission >650 nm.

732 **Synthesis of Bis[[N-(2-(pyridin-4-yl)ethyl)]-9,18-methano-1,8-**
733 **naphthalimido[b,f][1,5]diazocine (1).** Compound 3-Cl⁻ (0.303 g,
734 0.856 mmol) and paraformaldehyde (0.057 g, 1.89 mmol) were stirred
735 in trifluoroacetic acid (TFA) (6 mL) at 20 °C for 12 h under an argon
736 atmosphere. Excess TFA was removed under reduced pressure in the
737 presence of an excess of CH₂Cl₂. The resulting yellow powder was
738 dissolved in CH₃CN and purified on silica gel using a mixture of
739 CH₃CN/H₂O/NaNO₃ saturated (88:10:2) as the eluent. The product
740 was precipitated as its PF₆⁻ salt using ammonium hexafluorophos-
741 phate. The PF₆⁻ salt was dissolved in a minimum amount of MeOH
742 and treated with Amberlite IRA 400 (Cl) ion-exchange resin to
743 convert the product into the chloride form. The product was obtained
744 as a yellow solid after removal of MeOH under reduced pressure in
745 57% yield (0.18 g): mp dec above 235 °C; HRMS (MALDI) found
746 707.2169 ([M + Cl]⁺, C₄₁H₃₂N₆O₄Cl requires 707.2174); δ_{H} (600
747 MHz, DMSO-*d*₆) 9.15 (4H, d, *J* = 6 Hz, Py-H16, Py-H16'), 8.73 (2H,
748 d, *J* = 8.4 Hz, Ar-H5, Ar-H5'), 8.57 (2H, t, *J* = 7.9 Hz, Py-H17, Py-
749 H17'), 8.40 (2H, d, *J* = 8.0 Hz, Ar-H7, Ar-H7'), 8.05 (4H, t, *J* = 6.0
750 Hz, Py-H16, Py-H16'), 8.00 (2H, s, Ar-H2, Ar-H2'), 7.96 (2H, t, *J* =
751 8.0 Hz, Ar-H6, Ar-H6'), 5.16 (2H, d, *J* = 17.5 Hz, Ar-CH₂N), 4.95 and
752 4.92 (4H, dt, *J* = 14.0 Hz and *J* = 7.5 Hz, CH₂, H14, H14'), 4.71 (2H,
753 s, NCH₂N), 4.62 (2H, d, *J* = 17.5 Hz, Ar-CH₂N), 4.55 (4H, t, *J* = 7.0
754 Hz, CH₂, H13, H13'); δ_{C} (150 MHz), 163.7 (C=O), 163.1 (C=O),
755 149.3 (C), 145.9 (CH), 145.4 (CH), 130.7 (CH), 130.4 (CH), 129.4
756 (CH), 127.8 (CH), 127.6 (C), 127.2 (CH), 126.7 (C), 126.1 (C),
757 122.2 (C), 117.3 (C), 65.9 (CH₂), 59.6 (CH₂), 56.7 (CH₂), 40.7
758 (CH₂); ν_{max} (neat sample)/cm⁻¹ 3374, 1694, 1653, 1595, 1570, 1489,
759 1459, 1402, 1374, 1354, 1340, 1302, 1258, 1236, 1169, 925, 784.

760 **Synthesis of Bis[[N-(2-(methylpyridin-1-ium)ethyl)]-9,18-metha-**
761 **no-1,8-naphthalimido[b,f][1,5]diazocine (2).** Compound 4-PF₆⁻
762 salt (0.3014 g, 0.631 mmol) and paraformaldehyde (0.054 g, 1.79
763 mmol) were suspended in TFA and stirred at 20 °C for 12 h under an
764 argon atmosphere. The excess TFA was then removed under reduced
765 pressure in the presence of an excess of DCM. The resulting yellow
766 powder was dissolved in water and purified on silica gel using a
767 mixture of CH₃CN/H₂O/NaNO₃ saturated (80:18:2) as the eluent.
768 The product was precipitated as a PF₆⁻ salt using ammonium
769 hexafluorophosphate. The PF₆⁻ salt was dissolved in a minimum
770 amount of MeOH and treated with Amberlite IRA 400 (Cl) ion-
771 exchange resin to convert the product into the chloride form. The
772 product was obtained as a yellow solid in 53% yield (0.13 g, 0.168
773 mmol) after removal of excess MeOH under reduced pressure: mp dec
774 above 175 °C; HRMS (MALDI) found 700.2794 ([M]⁺, C₄₃H₃₆N₆O₄
775 requires 700.2798); δ_{H} (600 MHz, CD₃CN), 8.73 (2H, d, *J* = 8.3 Hz,
776 Ar-H5, Ar-H5'), 8.47 (2H, d, *J* = 8.0 Hz, Ar-H7, Ar-H7'), 8.46 (4H, d,
777 *J* = 6.0 Hz, Py-H17, Py-17'), 8.03 (2H, s, Ar-H2, Ar-H2'), 7.90 (4H, d,
778 *J* = 6 Hz, Py-H16, H16'), 7.89 (2H, t, *J* = 8.2 Hz, Ar-H6, Ar-H6'), 5.14
779 (2H, d, *J* = 17.4 Hz, Ar-CH₂N), 4.67 (2H, s, NCH₂N), 4.63 (2H, d, *J*
780 = 17.4 Hz, Ar-CH₂N), 4.38 and 4.36 (4H, dt, *J* = 14.0 Hz and *J* = 7.0
781 Hz, CH₂, H13, H13'), 4.23 (6H, s, CH₃), 3.27 (4H, t, *J* = 7.0 Hz, CH₂,
782 H14, H14'); δ_{C} (150 MHz) 164.9 (C=O), 164.3 (C=O), 160.9 (C),

150.5 (C), 145.4 (CH), 131.5 (CH), 131.4 (CH), 130.3 (CH), 129.3
(CH), 128.9 (C), 128.3 (C), 128.0 (CH), 127.0 (C), 123.7 (C), 119.2
(C), 67.2 (CH₂), 57.7 (CH₂), 48.6 (CH₃), 40.2 (CH₂), 34.6 (CH₂);
785 ν_{max} (neat sample)/cm⁻¹ 3376, 1692, 1647, 1595, 1571, 1459, 1402,
786 1372, 1339, 1302, 1257, 1231, 1187, 920, 786.

787
788 **Synthesis of Bis[[N-(2-(pyridin-4-yl)ethyl)]-9,18-methano-1,8-**
789 **naphthalimido[b,f][1,5]diazocine (5).** Compound 5 (0.25 g, 0.788
790 mmol) and paraformaldehyde (0.048 g, 1.59 mmol) were suspended
791 in TFA and stirred at 20 °C for 12 h under an argon atmosphere. The
792 excess TFA was then removed under reduced pressure in the presence
793 of an excess of CH₂Cl₂. The resulting crude product was purified by
794 trituration with methanol resulting in a yellow powder in 60% (0.158
795 g) yield: mp dec above 252 °C; HRMS (ESI) found 671.2407 ([M +
796 H], C₄₁H₃₁N₆O₄ requires 671.2407); δ_{H} (600 MHz, CDCl₃), 8.73
797 (2H, d, *J* = 8.5 Hz, Ar-H5, Ar-H5'), 8.62 (2H, d, *J* = 8.0 Hz, Ar-H7, Ar-
798 H7'), 8.49 (4H, d, *J* = 6.0 Hz, Py-H17, Py-17'), 8.09 (2H, s, Ar-H2,
799 Ar-H2'), 7.90 (2H, t, *J* = 8.0 Hz, Ar-H6, H6'), 7.26 (4H, d, *J* = 6.0 Hz,
800 Py-H16, Py-H16'), 5.18 (2H, d, *J* = 17.4 Hz, Ar-CH₂N), 4.70 (2H, s,
801 NCH₂N), 4.62 (2H, d, *J* = 17.4 Hz, Ar-CH₂N), 4.39 (4H, m, CH₂,
802 H13, H13'), 3.02 (4H, t, *J* = 7.0 Hz, CH₂, H14, H14'); δ_{C} (150 MHz):
803 163.8 (C=O), 163.2 (C=O), 149.2 (C), 149.1 (CH), 148.0 (C),
804 131.0 (CH), 130.5 (CH), 128.9 (CH), 128.2 (C), 127.2 (C), 127.1
805 (CH), 125.2 (C), 124.4 (CH), 122.8 (C), 118.4 (C), 69.9 (CH₂), 57.0
806 (CH₂), 40.1 (CH₂), 33.4 (CH₂); ν_{max} (neat sample)/cm⁻¹ 3058, 2953,
807 2923, 1689, 1656, 1596, 1570, 1510, 1459, 1440, 1372, 1301, 1255,
808 1232, 1169, 920, 786.

■ ASSOCIATED CONTENT

📄 Supporting Information

NMR and X-ray characterization, UV/vis, fluorescence, and CD
spectroscopy, DNA binding studies using UV/vis titration, CD,
LD, EtBr displacement assay, thermal melting, DNA photo-
cleavage, cellular uptake, and viability assay. This material is
available free of charge via the Internet at <http://pubs.acs.org>.

■ AUTHOR INFORMATION

Corresponding Authors

*E-mail: jmkelly@tcd.ie.

*E-mail: gunnlaut@tcd.ie.

Notes

The authors declare no competing financial interest.

■ ACKNOWLEDGMENTS

We thank Science Foundation Ireland (SFI: RFP 2006, RFP
2009, and PI 2010 grants), CSCB, and HEA PRTL Cycle 4 for
financial support. We also thank the Ministerio of Economía y
Competitividad of Spain for the funding of a postdoctoral
fellowship (to M.M.C.) and thank Trinity College Dublin for a
postgraduate studentship (S.B.). We thank Drs. John O'Brien,
Manuel Ruether, and Martin Feeney for help with NMR and
mass spectrometry studies. Finally, we thank Dr. Emma B.
Veale for her continuous support and help during this work and
for introducing the naphthalimide-based Tröger's bases as a
research theme into our laboratory. Her massive contribution
has and continues to greatly enrich our research endeavors.

■ REFERENCES

- (1) (a) Rúnarsson, Ö. V.; Artacho, J.; Wärnmark, K. *Eur. J. Org. Chem.* **2012**, 2012, 7015. (b) Dolenský, B.; Havlík, M.; Král, V. *Chem. Soc. Rev.* **2012**, 41, 3839. (c) Valík, M.; Strongin, R. M.; Král, V. *Supramol. Chem.* **2005**, 17, 347. (d) Dolenský, B.; Elguero, J.; Král, V.; Pardo, C.; Valík, M. *Adv. Heterocycl. Chem.* **2007**, 93, 1. (e) Bag, B. G. *Curr. Sci.* **1995**, 68, 279. (f) Spielman, M. A. *J. Am. Chem. Soc.* **1935**, 57, 583. (g) Tröger, J. *J. Prakt. Chem.* **1887**, 36, 225.

- 843 (2) (a) Wilcox, C. S. *Tetrahedron Lett.* **1985**, 26, 5749. (b) Webb, T.
844 H.; Suh, H.; Wilcox, C. S. *J. Am. Chem. Soc.* **1991**, 113, 8554. (c) Bag,
845 B. G.; Maitra, U. *Synth. Commun.* **1995**, 25, 1849.
- 846 (3) (a) Gardarsson, H.; Schweizer, W. B.; Trapp, N.; Diederich, F.
847 *Chem.—Eur. J.* **2014**, 20, 4608. (b) Paliwal, S.; Geib, S.; Wilcox, C. S. *J.*
848 *Am. Chem. Soc.* **1994**, 116, 4497. (c) Fischer, F. R.; Schweizer, W. B.;
849 Diederich, F. *Angew. Chem., Int. Ed.* **2007**, 46, 8270. (d) Hof, F.;
850 Scofield, D. M.; Schweizer, W. B.; Diederich, F. *Angew. Chem., Int. Ed.*
851 **2004**, 43, 5056.
- 852 (4) (a) Wilcox, C. S.; Adrian, J. C.; Webb, T. H.; Zawacki, F. J. *J. Am.*
853 *Chem. Soc.* **1992**, 114, 10189. (b) Cowart, M. D.; Sucholeiki, I.;
854 Bukownik, R. R.; Wilcox, C. S. *J. Am. Chem. Soc.* **1988**, 110, 6204.
- 855 (5) (a) Manjula, A.; Nagarajan, M. *Tetrahedron* **1997**, 53, 11859.
856 (b) Kim, K.; Choe, J. I. *Bull. Korean Chem. Soc.* **2006**, 27, 1737.
857 (c) Boyle, E. M.; Comby, S.; Molloy, J. K.; Gunnlaugsson, T. *J. Org.*
858 *Chem.* **2013**, 78, 8312.
- 859 (6) (a) Satishkumar, S.; Periasamy, M. *Tetrahedron: Asymmetry* **2009**,
860 20, 2257. (b) Kobayashi, T.; Moriwaki, T. *Heterocycles* **2004**, 62, 399.
861 (c) Goswami, S.; Ghosh, K.; Dasgupta, S. *J. Org. Chem.* **2000**, 65, 1907.
862 (7) (a) Hawes, C. S.; Fitchett, C. M.; Batten, S. R.; Kruger, P. E.
863 *Inorg. Chim. Acta* **2012**, 389, 112. (b) Weilandt, T.; Kiehne, U.;
864 Bunzen, J.; Schnakenburg, G.; Lutzen, A. *Chem.—Eur. J.* **2010**, 16,
865 2418. (c) Favera, N. D.; Kiehne, U.; Bunzen, J.; Hytteballe, S.; Lutzen,
866 A.; Piguet, C. *Angew. Chem., Int. Ed.* **2010**, 49, 125. (d) Weilandt, T.;
867 Kiehne, U.; Schnakenburg, G.; Lutzen, A. *Chem. Commun.* **2009**, 2320.
868 (e) Kiehne, U.; Weilandt, T.; Lutzen, A. *Eur. J. Org. Chem.* **2008**, 2056.
869 (f) Kiehne, U.; Weilandt, T.; Lutzen, A. *Org. Lett.* **2007**, 9, 1283.
- 870 (8) (a) Parchansky, V.; Matejka, P.; Dolensky, B.; Havlik, M.; Bour,
871 P. J. *Mol. Struct.* **2009**, 934, 117. (b) Havlík, M.; Král, V.; Kaplanek, R.;
872 Dolenský, B. *Org. Lett.* **2008**, 10, 4767. (c) Yuan, C. X.; Xin, Q. A.; Liu,
873 H. J.; Wang, L.; Jiang, M. H.; Tao, X. T. *Sci. China Chem.* **2011**, 54,
874 587.
- 875 (9) Recent examples include: (a) Kamiyama, T.; Ozer, M. S.; Otth,
876 E.; Deska, J.; Cvengros, J. *ChemPlusChem.* **2013**, 75, 1510. (b) Meyer-
877 Eppler, G.; Vogelsang, E.; Benkhauser, C.; Schneider, A.;
878 Schnakenburg, G.; Lutzen, A. *Eur. J. Org. Chem.* **2013**, 4523.
879 (c) Dolenský, B.; Kessler, J.; Jakubek, M.; Havlík, M.; Čejka, J.;
880 Novotná, J.; Král, V. *Tetrahedron Lett.* **2013**, 54, 308. (d) Benkhauser-
881 Schunk, C.; Wezlska, B.; Urbahn, K.; Kiehne, U.; Daniels, J.;
882 Schnakenburg, G.; Neese, F.; Lutzen, A. *ChemPlusChem* **2012**, 77, 396.
883 (10) Greenberg, A.; Molinaro, N.; Lang, M. J. *Org. Chem.* **1984**, 49,
884 1127.
- 885 (11) (a) Hamada, Y.; Mukai, S. *Tetrahedron: Asymmetry* **1996**, 7,
886 2671. (b) Tálás, E.; Margitfalvi, J.; Machytka, D.; Czugler, M.
887 *Tetrahedron: Asymmetry* **1998**, 9, 4151.
- 888 (12) (a) Tatibouet, A.; Demeunynck, M.; Andraud, C.; Collet, A.;
889 Lhomme, J. *Chem. Commun.* **1999**, 161. (b) Satishkumar, S.;
890 Periasamy, M. *Tetrahedron: Asymmetry* **2006**, 17, 1116.
- 891 (13) (a) Ikai, T.; Yamamoto, C.; Kamigaito, M.; Okamoto, Y.
892 *Chirality* **2005**, 17, 299. (b) Didier, D.; Tylleman, B.; Lambert, N.;
893 Vande Velde, C. M. L.; Blockhuys, F.; Collas, A.; Sergeev, S.
894 *Tetrahedron* **2008**, 64, 6252. (c) Kiehne, U.; Bruhn, T.; Schnakenburg,
895 G.; Fröhlich, R.; Bringmann, G.; Lützen, A. *Chem.—Eur. J.* **2008**, 14,
896 4246. (d) Sergeev, S.; Diederich, F. *Angew. Chem., Int. Ed.* **2004**, 43,
897 1738.
- 898 (14) Yashima, E.; Akashi, M.; Miyauchi, N. *Chem. Lett.* **1991**, 1017.
899 (15) (a) Bailly, C.; Laine, W.; Demeunynck, M.; Lhomme, J. *Biochem.*
900 *Biophys. Res. Commun.* **2000**, 273, 681. (b) Baldeyrou, B.; Tardy, C.;
901 Bailly, C.; Colson, P.; Houssier, C.; Charmantray, F.; Demeunynck, M.
902 *Eur. J. Med. Chem.* **2002**, 37, 315.
- 903 (16) Paul, A.; Maji, B.; Misra, S. K.; Jain, A. K.; Muniyappa, K.;
904 Bhattacharya, S. *J. Med. Chem.* **2012**, 55, 7460.
- 905 (17) (a) Ezadyar, S. A.; Kumbhar, A. S.; Kumbhar, A. A.; Khan, A.
906 *Polyhedron* **2012**, 36, 45. (b) Claessens, N.; Pierard, F.; Bresson, C.;
907 Moucheron, C.; Kirsch-De Mesmaeker, A. *J. Inorg. Biochem.* **2007**, 101,
908 987. (c) Bresson, C.; Luhmer, M.; Demeunynck, M.; Kirsch-De
909 Mesmaeker, A.; Pierard, F. *Tetrahedron Lett.* **2004**, 45, 2863.
- 910 (18) (a) Banerjee, S.; Veale, E. B.; Phelan, C. M.; Murphy, S. A.;
911 Tocci, G. M.; Gillespie, L. J.; Frimannsson, D. O.; Kelly, J. M.;
Gunnlaugsson, T. *Chem. Soc. Rev.* **2013**, 42, 1601. (b) Lee, M. H.; 912
Jeon, H. M.; Han, J. H.; Park, N.; Kang, C.; Sessler, J. L.; Kim, J. S. J. 913
Am. Chem. Soc. **2014**, 136, 8430. (c) Yang, Q.; Yang, P.; Qian, X.; 914
Tong, L. *Bioorg. Med. Chem. Lett.* **2008**, 18, 6210. (d) Xie, S.-Q.; 915
Zhang, Y.-H.; Li, Q.; Xu, F.-H.; Miao, J.-W.; Zhao, J.; Wang, C.-J. 916
Apoptosis **2012**, 17, 725. (e) Kilpin, K. J.; Clavel, C. M.; Edfafe, F.; 917
Dyson, P. J. *Organometallics* **2012**, 31, 7031. (f) Wu, X.; Sun, X.; Guo, 918
Z.; Tang, J.; Shen, Y.; James, T. D.; Tian, H.; Zhu, W. J. *Am. Chem. Soc.* 919
2014, 136, 3579. (g) Hettiarachchi, S. U.; Prasai, B.; McCarley, R. L. J. 920
Am. Chem. Soc. **2014**, 136, 7575. (h) Silvers, W. C.; Prasai, B.; Burk, D. 921
H.; Brown, M. L.; McCarley, R. L. *J. Am. Chem. Soc.* **2013**, 135, 309. 922
(i) Lee, M. H.; Kim, J. Y.; Han, J. H.; Bhuniya, S.; Sessler, J. L.; Kang, 923
C.; Kim, J. S. *J. Am. Chem. Soc.* **2013**, 134, 12668. (j) Braña, M. F.; 924
Cacho, M.; Garcia, M. A.; de Pascual-Teresa, B.; Ramos, A.; Acero, N.; 925
Llinares, F.; Munoz-Mingarro, D.; Abradelo, C.; Rey-Stolle, M. F.; 926
Yuste, M. J. *Med. Chem.* **2002**, 45, 5813.
- (19) Examples of DNA targeting agents include: (a) Banerjee, S.; 927
Kitchen, J. A.; Gunnlaugsson, T.; Kelly, J. M. *Org. Biomol. Chem.* **2013**, 928
11, 5642. (b) Banerjee, S.; Kitchen, J. A.; Gunnlaugsson, T.; Kelly, J. 929
M. *Org. Biomol. Chem.* **2012**, 10, 3033. (c) Ryan, G. J.; Elmes, R. B. P.; 930
Quinn, S. J.; Gunnlaugsson, T. *Supramol. Chem.* **2012**, 24, 175. 931
(d) Ryan, G. J.; Quinn, S.; Gunnlaugsson, T. *Inorg. Chem.* **2007**, 47, 932
401. Examples of luminescent and colorimetric sensors include: 933
(e) Veale, E. B.; Tocci, G. M.; Pfeffer, F. M.; Kruger, P. E.; 934
Gunnlaugsson, T. *Org. Biomol. Chem.* **2009**, 7, 3447. (f) Duke, R. M.; 935
Gunnlaugsson, T. *Tetrahedron Lett.* **2007**, 48, 8043. (g) Duke, R. M.; 936
Gunnlaugsson, T. *Tetrahedron Lett.* **2011**, 52, 1503. (h) Ali, H. D. P.; 937
Kruger, P. E.; Gunnlaugsson, T. *New J. Chem.* **2008**, 32, 1153. 938
(i) Kitchen, J. A.; Martinho, P. N.; Morgan, G. G.; Gunnlaugsson, T. 939
Dalton Trans. **2014**, 43, 6468. 940
- (20) (a) Veale, E. B.; Frimannsson, D. O.; Lawler, M.; Gunnlaugsson, 941
T. *Org. Lett.* **2009**, 11, 4040. (b) Veale, E. B.; Gunnlaugsson, T. *J. Org.* 942
Chem. **2010**, 75, 5513. 943
(21) Elmes, R. B. P.; Erby, M.; Bright, S. A.; Williams, D. C.; 944
Gunnlaugsson, T. *Chem. Commun.* **2012**, 48, 2588. 945
(22) Duke, R. M.; Veale, E. B.; Pfeffer, F. M.; Kruger, P. E.; 946
Gunnlaugsson, T. *Chem. Soc. Rev.* **2010**, 39, 3936. 947
(23) (a) Fletcher, N. C.; Keene, F. R. *J. Chem. Soc., Dalton Trans.* 948
1999, 683. (b) Fletcher, N. C.; Junk, P. C.; Reitsma, D. A.; Keene, F. 949
R. J. Chem. Soc., Dalton Trans. **1998**, 133. 950
(24) Deprez, N. R.; McNitt, K. A.; Petersen, M. E.; Brown, R. G.; 951
Lewis, D. E. *Tetrahedron Lett.* **2005**, 46, 2149. 952
(25) (a) Yuan, C. X.; Tao, X. T.; Wang, L.; Yang, J. X.; Jiang, M. H. *J.* 953
Phys. Chem. C **2009**, 113, 6809. (b) Yuan, C. X.; Tao, X. T.; Ren, Y.; 954
Li, Y.; Yang, J. X.; Yu, W. T.; Wang, L.; Jiang, M. H. *J. Phys. Chem. C* 955
2007, 111, 12811. 956
(26) Carter, M. T.; Rodriguez, M.; Bard, A. J. *J. Am. Chem. Soc.* **1989**, 957
111, 8901. 958
(27) McGhee, J. D.; von Hippel, P. H. *J. Mol. Biol.* **1974**, 86, 469. 959
(28) (a) Wilson, W. R.; Baguley, B. C.; Wakelin, L. P. G.; Waring, M. 960
Mol. Pharmacol. **1981**, 20, 404. (b) Baguley, B. C.; Denny, W. A.; 961
Atwell, G. J.; Cain, B. F. *J. Med. Chem.* **1981**, 24, 170. 962
(29) Vasudevan, S.; Smith, J. A.; Wojdyla, M.; McCabe, T.; Fletcher, 963
N. C.; Quinn, S. J.; Kelly, J. M. *Dalton Trans.* **2010**, 39, 3990. 964
(30) Dai, Q.; Xu, C.-Y.; Sato, Y.; Yoshimoto, K.; Nishizawa, S.; 965
Teramae, N. *Anal. Sci.* **2006**, 22, 201. 966
(31) Sato, Y.; Nishizawa, S.; Yoshimoto, K.; Seino, T.; Ichihashi, T.; 967
Morita, K.; Teramae, N. *Nucleic Acids Res.* **2009**, 37, 1411. 968
(32) (a) Sowers, L. C.; Shaw, B. R.; Sedwick, W. D. *Biochem. Biophys.* 969
Res. Commun. **1987**, 148, 790. (b) Wang, S.; Kool, E. T. *Biochemistry* 970
1995, 34, 4125. 971
(33) Fairley, T. A.; Tidwell, R. R.; Donkor, I.; Naiman, N. A.; 972
Ohemeng, K. A.; Lombardy, R. J.; Bentley, J. A.; Cory, M. *J. Med.* 973
Chem. **1993**, 36, 1746. 974
(34) Boger, D. L.; Fink, B. E.; Brunette, S. R.; Tse, W. C.; Hedrick, 975
M. P. *J. Am. Chem. Soc.* **2001**, 123, 5878. 976
(35) Nordén, B.; Rodger, A.; Dafforn, T. *Linear Dichroism and* 977
Circular Dichroism; The Royal Society of Chemistry: London, 2010. 978
979

- 980 (36) Hiort, C.; Lincoln, P.; Norden, B. *J. Am. Chem. Soc.* **1993**, *115*,
981 3448.
- 982 (37) Rogers, J. E.; Abraham, B.; Rostkowski, A.; Kelly, L. A.
983 *Photochem. Photobiol.* **2001**, *74*, 521.
- 984 (38) Crosby, G. A.; Demas, J. N. *J. Phys. Chem.* **1971**, *75*, 991.
- 985 (39) Sheldrick, G. M. *Acta Crystallogr., Sect. A* **2008**, *A64*, 112.